EXO-200 Phase II α-decay Analysis with Machine Learning Reconstruction Techniques

Carson Lloyd
Advisor: Dr. Michelle Dolinski

Submitted in partial fulfillment
of the requirements for
the degree of Bachelor of Science in Physics

Drexel University, Philadelphia, PA

May 11, 2018

Abstract

Neutrinos (low-mass neutral fermions) can be observed as products of beta decays. The not-yet-observed neutrinoless double beta decay ($0\nu\beta\beta$, lower limit $T_{1/2} = 1.8 \times 10^{25}$years) holds special interest due to its impact on our understanding of neutrinos and the Standard Model of particle physics.

The EXO-200 detector is a time projection chamber which collects ionization and scintillation signals from particle decays within a sample of liquid ^{136}Xe in hopes of witnessing $0\nu\beta\beta$. In such a sensitive experiment, α particles from contaminants need to be well-understood in order to characterize their effects in the detector itself. α decays, though distinguishable by their unique footprint, can be missing full reconstruction data because of the detector's optimization for $0\nu\beta\beta$.

Machine learning allows us to use our knowledge of the decay chain of ^{222}Rn in combination with what fully reconstructed data there is to create decision tree regression models, which are used to predict the missing pieces that make α decay studies difficult. I use data from EXO-200 Phase II in combination with the machine learning algorithms to study drift velocities of ions and the surfaces of the detector. I find an ion drift velocity consistent with previous analysis and show the continued validity of this machine learning reconstruction method.

Contents

1 Background

1.1 Neutrinos

Neutrinos (ν) are fermions (elementary particles with half-integer spins), and are the least massive of the elementary particles. Neutrinos are also hugely abundant in the Universe - the neutrino flux on Earth from our Sun alone is about 65 billion per cm^2 per second. There are three flavors of neutrinos and their antineutrino partners: electron (ν_e), mu (ν_μ), and tau (ν_τ). As their name predicts, they are electrically neutral. Neutrinos only interact via the weak force and gravitational force; as both of these forces are extremely small in magnitude, and because the neutrino's mass is so low and most travel at very high speeds, they rarely interact with other matter in the Universe - and thus are difficult to study.

The neutral characteristic of the neutrino, its weak interactions, and the sheer number of them make it an interesting and important particle. In physics research alone, these properties of neutrinos make them useful for studying objects and events very far away in distance and time. The more we know about neutrinos, the more they can be used to explain the Standard Model of particle physics. Since the discovery in 1998 that neutrinos are not massless (after particle physics and the Standard Model predicted a zero-mass particle), one of the most important questions about neutrinos has been how they acquire that mass. Neutrinos are being studied in many observational experiments today, in the hopes that they will be able to explain this problem in the Standard Model.

Because neutrinos are difficult to detect directly, β decays are the focus of the detection search. The electrons that are released are easier to detect with little more than a stable and uniform electric field and a wire mesh for collection. A standard β decay involves a neutron decaying to a proton, with the release of an $e^- + \overline{\nu}_e$ pair (electron and anti-electron neutrino). A related decay that has been observed is a double beta decay ($2\nu\beta\beta$) [1]: two simultaneous β decays where the products are two neutrinos and two β particles. The current limit on the 2 neutrino double beta decay's half-life is over 2×10^{21} years [21] (at least 10^{11} times the age of the Universe).

1.2 $0\nu\beta\beta$

There is a special type of double beta decay that many theorists expect to exist: neutrinoless double beta decay ($0\nu\beta\beta$). In this decay, two neutrinos are emitted only as virtual particles at the same time and two electrons are emitted with the full energy of the decay (Figure 1).

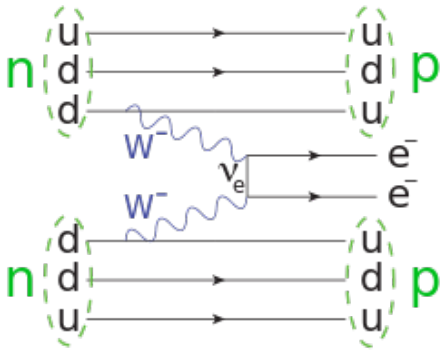

Figure 1: $0\nu\beta\beta$ Feynman Diagram [21]

The $0\nu\beta\beta$ is of special interest because it would show that the neutrino is its own antiparticle and obeys Majorana statistics, if observed. It would also provide a vehicle with which to constrain the absolute neutrino mass scale, or at least allow a better limit on the half-life for this decay (which also limits the neutrino mass scale).

To search for a rare decay mode, a detector must have a large sample size to increase statistics and have strong energy resolution in order to strike backgrounds. To illustrate this, Figure 2 demonstrates the energy resolution of EXO-200's detector, highlighting the energy range around the Q-value for $2\nu\beta\beta$ decays in ^{136}Xe - 2457.83 keV. [15]

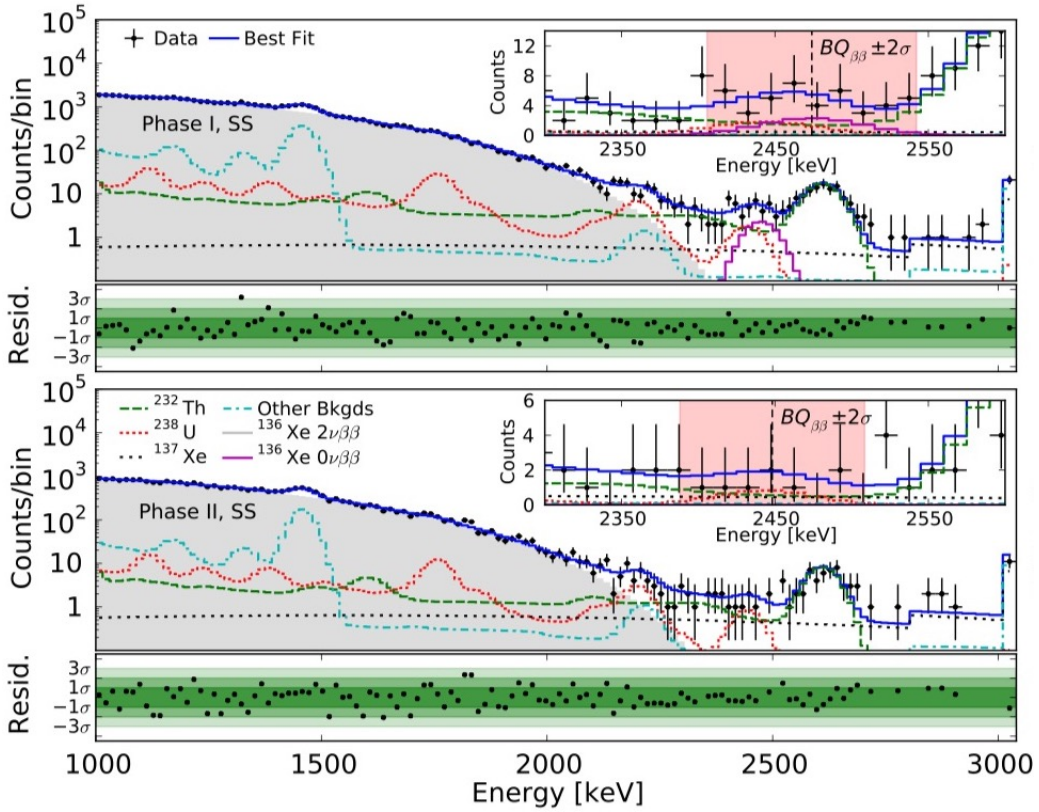

Figure 2: EXO-200 Best fit over low background data energy spectrum for Phase I (top) and Phase II (bottom). [4]

Most importantly, the peak around this Q value is distinguishable and above backgrounds.

2 EXO-200 and $0\nu\beta\beta$

The EXO-200 Collaboration attempts to detect this $0\nu\beta\beta$ decay. EXO (Enriched Xenon Observatory) is a detector experiment with a 200kg sample of liquid Xenon (LXe) enriched to 80% ^{136}Xe. This Xenon isotope does actively produce double beta decays [1], and produced the first $2\nu\beta\beta$ decay sighting at EXO-200.

The LXe sample is housed in a double time projection chamber (TPC) within a cryostat system (HFE7000 fluid) which is lead-shielded and 2150 ft. underground [9] at the Waste Isolation Pilot

Plant (WIPP) operated by the Department of Energy in Carlsbad, New Mexico.

It is imperative that backgrounds are kept to a minimum, because the rate of $0\nu\beta\beta$ is so low. A remote location deep underground is useful to both reduce the number of naturally occurring radioactive contaminants from Earth and to filter out many of the cosmic interferences that would be encountered on the surface. The TPC itself is also surrounded by a plastic scintillator muon veto which allows tagging of cosmogenic muons with over 96% efficiency. [3]

2.1 Double Time Projection Chamber

The EXO-200 detector is a double TPC cylinder, 40cm in diameter and 44cm in length. [1]

The apparatus is divided in half by a cathode grid and two parallel anode grids (one at each end). See Figure 3 (pg. 4) for a simple schematic of the TPC. These collect charge clusters from the decays. At both ends are also arrays of ~250 large area avalanche photodiodes (LAAPDs) which detect scintillation light. The cathode grid is 90% optically transparent and thus allows both LAAPDs to detect light from anywhere in the detector. [7] In addition to the field produced by the cathode and anodes, the entire TPC is surrounded by a field cage, which keep the interior field lines extremely uniform (to within 1% [1]).

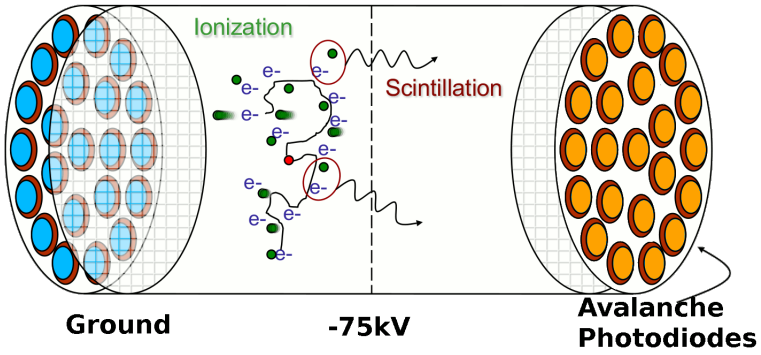

Figure 3: Time Projection Chamber [9]

When a decay event occurs in the LXe, the decay electrons ionize nearby Xe, and create an electron shower which drifts in the field of the detector. The uniform field inside the detector guides the electrons, and their collection gives a 2D position of the decay site. The decay electrons also excite some of the nearby atoms, which relax and release UV light that is collected on the photodiodes almost instantly. The time difference between these two signals allows the 3D position to be recreated. The energy of the event is related to the number of ionized electrons detected and also the amount of light received. By reconstructing these decays with both detection systems (scintillation and ionization), 3D position and energy measurements are recorded.

2.2 ^{136}Xe

Inside the detector, the LXe is kept at 167 K and 147 kPa. The pressure (about 1.5 standard atmospheric pressure at sea level) is easily obtainable within the apparatus, and the temperature is held by the cryostat.

^{136}Xe is a costly choice of material, but there are several properties that make it ideal for EXO-200 [7]. First, ^{136}Xe has a Q-value of 2457.8 keV for its $2\nu\beta\beta$ decay mode ($^{136}\text{Xe} \rightarrow {}^{136}\text{Ba}$). This energy is high enough that it excludes backgrounds of most radioactive decays. Second, the ^{136}Xe acts as both the decay source and detection medium, which increases sensitivity as well. Third, Xe being noble and a gas at standard temperature and pressure allows easy purification and enrichment processes, respectively. Last, all radioisotopes of Xe have short lifetimes and therefore the sample quickly de-contaminates itself.

These factors allow Xe to contribute little to no added background as the detection medium (and source) and facilitate maintenance operations.

2.3 EXO-200 Current State and Results-to-Date

The EXO-200 Collaboration reported the observation of the $2\nu\beta\beta$ decay in ^{136}Xe (2011) with

$$T_{1/2} = 2.11 \pm 0.04(stat.) \pm 0.21(sys.) \times 10^{21} \text{ years.}$$

This was the first of that decay mode to be detected in ^{136}Xe. [1]

With improvements in energy resolution and years'-worth more data, in 2014 the Collaboration improved their half-life sensitivity $T_{1/2} = 1.9 \times 10^{25}$ years. At this time, a lower limit on the half-life for $0\nu\beta\beta$ was presented at 90% confidence level:

$$T_{1/2} = 1.1 \times 10^{25} \text{years [5]}$$

Earlier this year (February 2018), the Collaboration published updated results which detailed major upgrades and improvements to the detector. Phase II data collection after the upgrades began in May 2016.

- Energy resolution improved (Figure 2, pg. 3) to

$$\sigma/E = 1.23\%$$

- Drift E-field increased by 50%, to 567 V/cm (cathode voltage, $V_C = -12kV$)
- Increased shielding to suppress Rn from cryostat
- Additional analysis techniques for $0\nu\beta\beta$ discrimination

These hardware and analysis upgrades led to a two-fold increase in their half-life sensitivity to 3.7×10^{25} years. With no evidence for $0\nu\beta\beta$, they presented an increase in the lower-limit on the $0\nu\beta\beta$ half-life as well:

$$T_{1/2} = 1.8 \times 10^{25} \text{years}$$

at the 90% confidence level. [6]

With these updates, it is worth a continuation and re-investigation of the studies done by Erica Smith in [16]. This is what I will present below.

3 α decays and Radon

Along with the ^{136}Xe in the detector, there are other radioactive isotopes from impurities. Impurities in the detector could come from any of the materials that make up the detector or could be brought in with the LXe after a drain and re-fill.

The most common of these impurities, because its half-life is almost 4 days, is ^{222}Rn, which is in the decay chain from Uranium. ^{222}Rn decays via α decay, and continues down a decay chain known as the Radon progeny which is very well understood (see Figure 4, pg. 6).

α decays involve an unstable nucleus emitting an α particle (two protons and two neutrons, He^{2+}). These α particles are unquestionably more massive compared to the β decay's electrons, and because of this they move slower.

The α decays have a low ionization signal due to their higher mass and therefore lower energies, and a higher scintillation signal. These differences make α decays easily distinguishable from β decays in the EXO-200 detector.

Unfortunately, "easily distinguishable" does not mean "easily reconstructed" in this case. Because the EXO-200 detector is optimized for a β decay search and will not see most α decay ionization signals, there is a specific trigger that looks for large α events (around 25,000 photons). Though the events in the detector can be determined to be α or β decays based mostly upon the scintillation signals, the low (and many times unnoticed) ionization signal is missing.

This ionization signal is where two dimensions of position data come from in the recreation of the event, and therefore it is difficult to fully reconstruct the α decays with the data from the detector. Many events are missing at least the x and y (radial) position measurements for decay events.

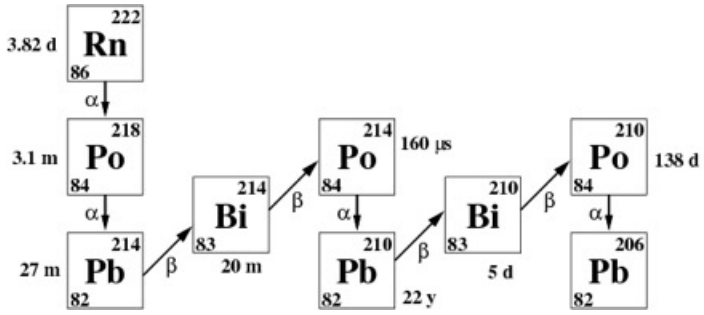

Figure 4: Radon Decay Progeny [10]

In the search for $0\nu\beta\beta$ decay, the EXO-200 TPC and detector need to be extremely sensitive and accurate. It is important to understand how the ^{222}Rn and other radioactive products decay inside the detector because they contribute to signal distractions during the search for $0\nu\beta\beta$. Those decays also give insight into how these α particles interact with the Teflon sides of the detector container. This interaction could charge the walls of the detector and cause ions to drift in unexpected ways.

Because the ^{222}Rn goes through a well-known decay chain with known lifetimes, we do have the ability to both use machine learning to study and reconstruct α decay events to some level of accuracy, and also study decay coincidences within the ^{222}Rn Progeny.

By studying these α decay events and their subsequent decays, and working on an algorithm to reconstruct them with more accuracy, we can begin to understand better how they affect the detector. This type of machine learning aided reconstruction and analysis can move forward as a proof-of-concept for future detectors, namely nEXO (next EXO).

I build on Erica Smith's work [16], with Phase II data below. By using a decision tree learning method, Python scikit-learn's DecisionTreeRegressor, we are able to reconstruct α decay events which do not have complete position reconstructions.

4 Data Selection

4.1 Data Retrieval and Preprocessing

The detector systems for EXO-200 save raw binary data. There are 226 hardware channels: 76 of each U- and V-wire signals (anode and induction, respectively) 74 APD gang signals, muon veto panel output, and a high voltage glitch detector. Data is recorded continuously at a rate of 0.1 Hz along with activity triggers for data collection: U-wire trigger for γ and β events ($\sim$ 100 keV), APD activity trigger, and overall APD signal sum trigger for α events ($\sim 25,000$ photons). [2] The raw data goes through a data processing pipeline which does the following [2]:

1. "Rootification" - convert binary to ROOT, low level verification of data validity
2. Reconstruction - make first-pass at noise identification, muon tagging, data extraction and classification
3. Process - finalize reconstruction, data corrections for known inaccuracies
4. Masking - blind all $0\nu\beta\beta$ candidates
5. "Finish Up" - run standard analysis scripts, useful for tracking trends over time
6. Denoising - improve fit to scintillation energy

More specifically, the reconstruction phase analyzes the raw waveforms and extracts specific parameters (amplitudes, times, etc.), while tagging noise events and performing some low level computations. In processing the data, the wire signals and APD signals are combined into charge and scintillation clusters, and those clusters are corrected for some detector inefficiencies, electron lifetimes, and position dependent light collection bias [12].

The entirety of the data that I analyzed in this work is from Phase II, and had gone through all of the pre-processing prior to my use of it.

4.2 α-decay Selection

α decays have a much different footprint than the β decays. As discussed above, the α decays show a low ionization signal and a higher scintillation signal, due to their larger ionization density and larger amount of recombination [4]. This can be seen clearly when plotting the energy of the decay versus the number of scintillation counts in the signal.

In Figure 5 (pg. 8), I plotted an unfiltered data set as a scatter plot, where each event's decay charge energy is posed against its number of scintillation signal counts. Overlaid in red are the decay events that pass the α selection cuts. This leaves the β decay events in the blue horizontal cluster. The two distinctly clustered populations are clear, and this justifies classification cuts that I apply and will detail later.

The green line represents

$$y = 33.864,$$

which will be discussed further below, but which clearly delineates a simple baseline cut between the masses of β and α decays.

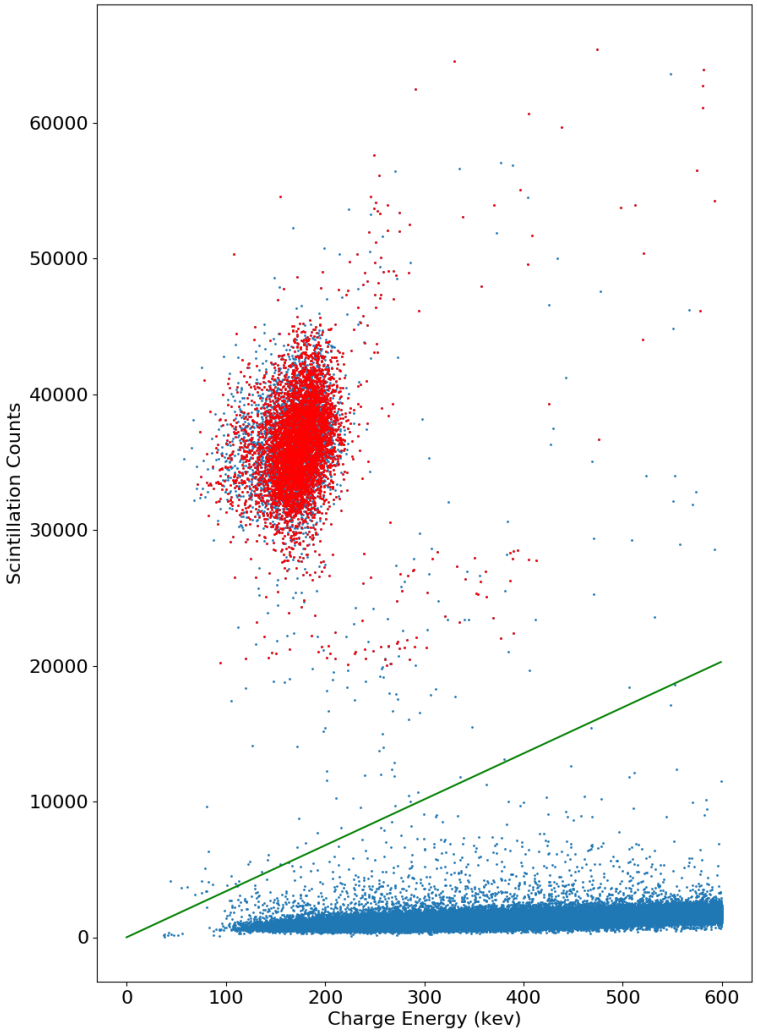

Figure 5: Energy v. Scintillation Counts, red events passing the α cuts

One should note that in Figure 5 (pg. 8), the "cloud" shaped region at the top-left is roughly bounded by 30,000-40,000 counts on the y-axis, and the flat cluster at the bottom of the figure is much below 10,000 counts on the y-axis. In the overlay, the single large cluster matches closely with the "cloud" shaped region in the first figure, whereas the flat cluster has been completely eliminated. I will present these cuts in more detail below.

4.3 Data Sets and Cuts

In the analysis in question, I am looking for α decay events in a detector optimized for β decays. This means that the best "runs" to use are Golden Masked runs (see Section 4, pg. 7).

As noted before, the data sets I used for analysis were all of type "Data-Physics," and of quality "Golden." When collecting the data sets they are forced through a set of initial cuts. Any events tagged as noise or tagged as a muon event are discarded. At this point the data sets are high quality without noise events, but include both β and α decays.

Once the data runs are compiled and cut into initial sets, I run them through another set of checks and possible cuts. The verifications are:

1. Total signal count on APD planes must be greater than 20,000
2. Must have a scintillation cluster
3. Cut events on the cathode or anodes
4. Cut events on the surface of detector
5. Must have charge cluster
6. Ratio of scintillation count and energy must be < 33.864

Items 3 and 4 in the list above together are referred to as the fiducial volume cut. This fiducial volume cut removes a vast majority of the events. See Figure 6 on page 10. This is for two reasons. First, many of the α decay events occur at the walls of the detector. The materials that make up the detector have more impurities in them, and therefore are much more likely to create α decays than the purified LXe. Second, the α particles do not travel very far, and thus the signals that are collected have usually originated from a locale near the detection planes. Event clustering near the cathode is especially expected, because charged particles will drift towards it and then decay. [16]

Specifically, I cut data sets down to 5,404 events from 48,748 events by applying the fiducial volume cut (this is a difference of 43,344 events, or 88.9% of the full set). Clearly, the events in the fiducial volume cut were made up a significant portion of the data.

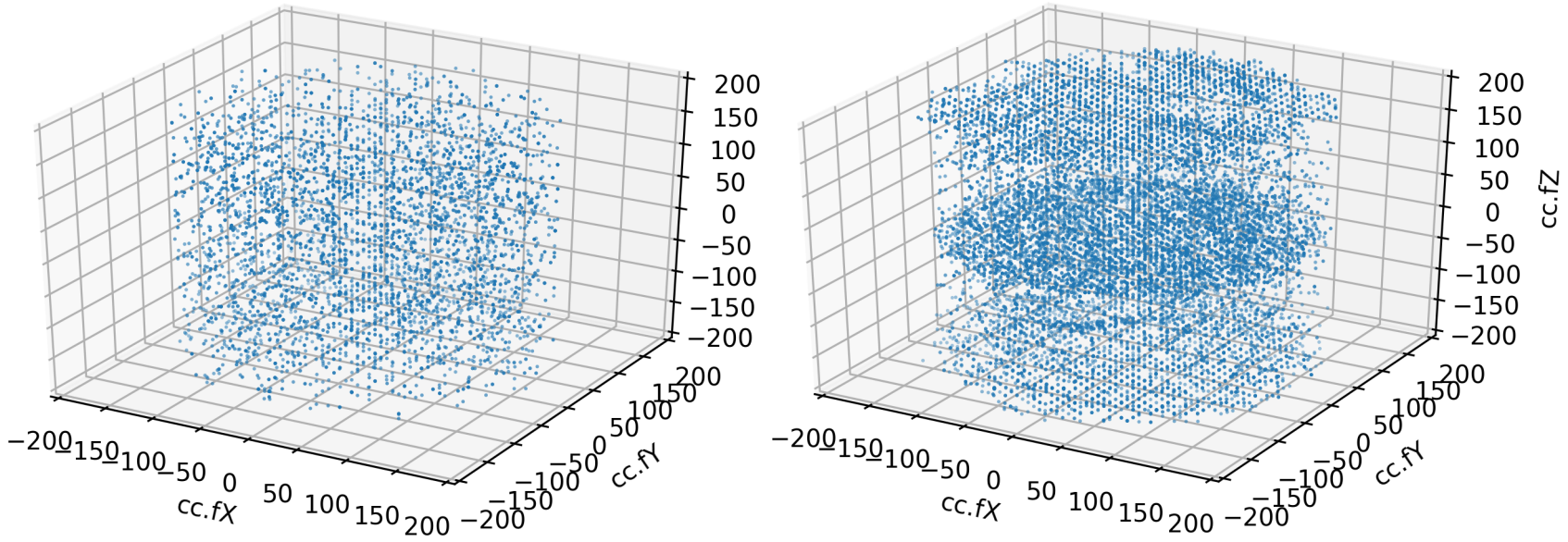

(a) With fiducial volume cut

(b) Without fiducial volume cut (all events)

Figure 6: Comparison of Event Positions with and without Fiducial Volume Cut

Table 1: Data Set Matrix

	Fiducial Volume Cut	Surviving Events	Total Events
Phase II		5,404	90,419
Phase II		48,748	

4.4 Formal Data Sets and Amounts of Data

Phase II is defined as data-runs (period of data collection) 7104-9097, though technically Phase II is defined as beginning in run 6385. This gap is due to an electronics upgrade and a change to the voltage of the cathode to -12 kV (see Section 2.3, pg. 5). Phase I is defined as runs 2464-6370. [13]

Table 1 details some statistics of the full data set I used. At the time of retrieval, I pulled $90,419$ events from Phase II, and the fiducial volume cut (green row) reduced the number of events to $5,404$.

5 Reconstructions

The reason for the machine learning is to have a method for reconstruction of events without a full position reconstruction. As discussed earlier (Section 3, pg. 6), this occurs especially frequently with α decays. This makes them a good target for reconstruction tests.

Once the data set of fully-reconstructed events is cut and saved, it can be used to train the decision tree. Files were saved with Python cPickle before transferring from the computing servers.

First, the entire data set needs to be split into training and testing sets. In this analysis, I take a training set of 30% and a testing set of 70%. Python scikit-learn's Cross-Validation 'train_test_split' method does this nicely. While preserving indexing in multiple arrays it will split testing and training data sets out from initial arrays. At this point, the training sets can be used to train the decision tree.

By removing position data from the testing set in order to test the trained decision tree, we are able to see how well our method is performing. When using the decision tree to reconstruct data, it outputs a score which is the "mean accuracy on the given test data." [22]

The Phase II data set that I used in the main analysis scored 0.931 (where a training set would score 1.0). This means that the reconstruction prediction on the test data was accurate according to the decision tree's self-scoring algorithm.

For a visual representation, see Figure 7 on page 12. This figure plots the differences between the predicted data sets and the original reconstructed data sets. This is possible because the "test" data sets are fully reconstructed events that have been redacted.

Since this tree is trained on fully reconstructed α events, any other similar data set (with similar cuts) should perform well under this reconstruction. This method is used later.

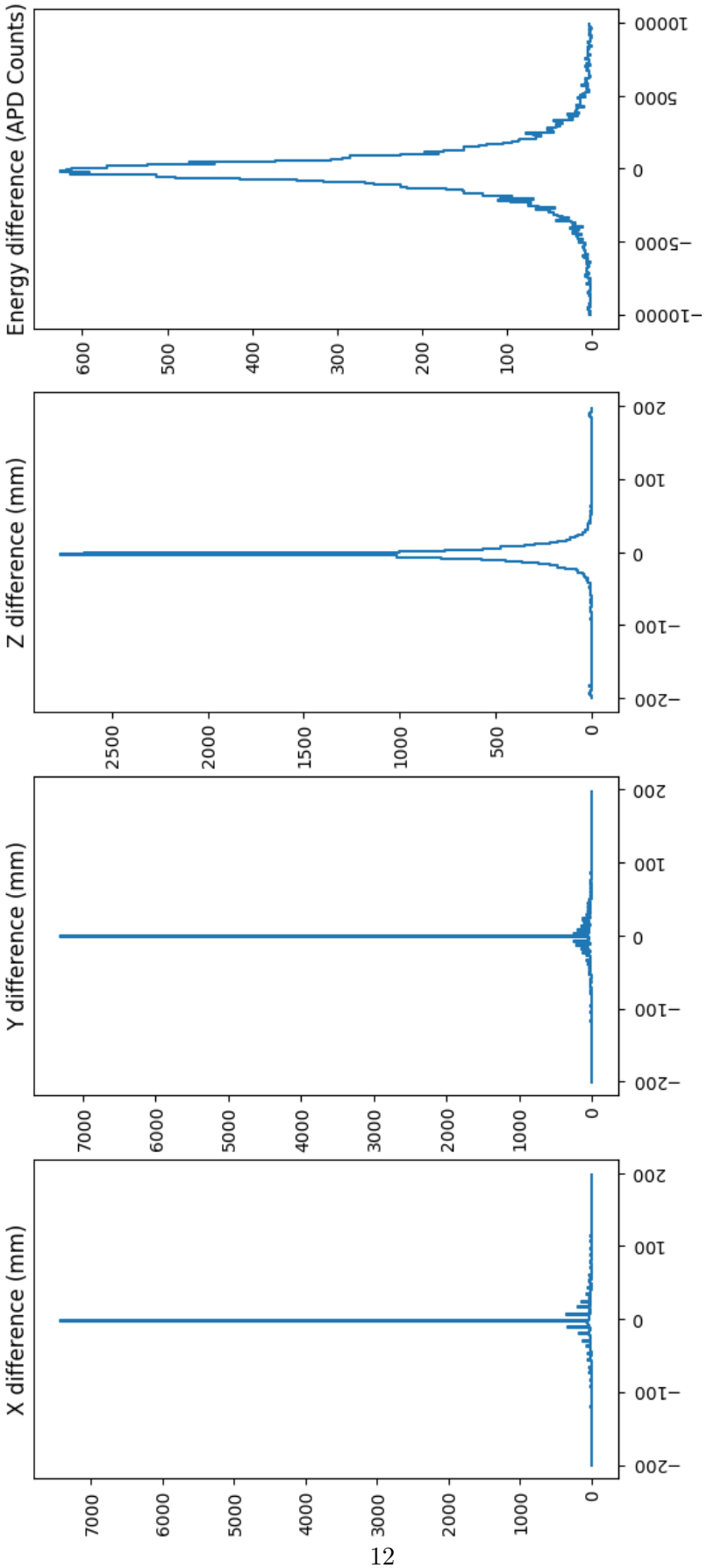

Figure 7: Differences comparing reconstructed test data to initial test data

6 Results

6.1 Ion Drift Time

6.1.1 Coincidence Selection

Coincidences denote two sequential decays, and importantly in this case, both in the Radon Progeny decay chain. Because the Radon Progeny is well known, we can tag decay coincidences by performing some simple cuts and checks to the data. In this coincidence study, we focus on ^{222}Rn and ^{218}Po, because of the short half-life (3.1 minutes), which makes it easy to associate the decays with few false coincidences. This is also an $\alpha - \alpha$ coincidence, which makes it easier to study within this activity as a whole.

To associate the coincidences, we apply certain filters to each pair of events in event-time order. First, we require that δt between the two events in the coincidence be $\leq$ 180s. This is because the lifetime of ^{222}Rn decaying into ^{218}Po is within this timeframe. This is also one of the largest guards against tagging false coincidences.

Next, we restrict the events to be detected within one U-wire away from each other, because they are not expected to drift far apart radially. This cut amounts to a $\delta U \leq$ 9.0mm, which is the spacing between U-wires. Finally, we restrict the 2D (x and y, radial) change in position to be $\leq$ 30.0mm. [4]

As less intensive data checks, we also require $\delta t \geq 0.0$ and that the two events occur on the same half of the detector.

6.1.2 Plots and Results

In Figure 8 (pg. 16) I show ^{218}Po drift time versus drift distance. In the center ($z = 0$) there is a vertical population of neutral ^{218}Po which do not drift much before decaying. There should be a prominent positive-sloped population from $z = 0$, which would indicate ^{218}Po ions which are drifting in the electric field towards the cathode. Due to the lack of events surviving the cuts from Phase II, there is not a prominent feature here, though there may be the beginnings of a drifting population. In contrast, see Figure 9 (pg. 16), which is the original version of the plot from [16].

Though there is not a strong drifting population, I do present a peak in coincidences with drift velocities that match closely to Smith's in [16]. See Figure 10 (pg. 17). The ion drift velocity peak is present at:

$$v = 1.053 \text{ mm/s}.$$

This is similar to the drift velocity that Smith presented:

$$v = 1.153 \pm 0.42 \text{ mm/s}.$$

When I cut all data points that are not within the general bounds of the ion drift peak, the Gaussian fit yields a lower value, though it should be noted that this peak only contains six coincidences.

In Figure 11 (pg. 18) I show ^{218}Po drift time versus drift velocity. Once again, my event count is low in Phase II, so I have attached the corresponding plot from [16].

6.1.3 Conclusion

The ion velocity peak at

$$v = 1.053 \text{ mm/s}$$

Table 2: Raw Counts for 0CC and 1CC Events, Compared to Smith [16]

	1CC			**0CC**		
	Counts	Percent	Phase I Percent	Counts	Percent	Phase I Percent
$R > 172$ mm	0	0%	2.1%	0	0%	16.3%
$R < 172$mm	60,371	100%	96.8%	2147168	100%	83.7%
outside fiducial z	12850	21.3%	29.7%	2068267	96.3%	31.6%
$20 <\mid z \mid < 172$ mm	47521	78.7%	69.2%	78901	3.7%	68.4%
$20 <\mid z \mid < 172$ mm & R >172 mm	0	0%	1.8%	0	0%	14.1%
Total	60371			2147168		

is compelling, especially as it seems to be similar to Smith's. [16] All of the drift time analyses would benefit greatly from more data. There are too few events to draw conclusions from.

In the end, we would expect some variance caused by the increase in the electric field strength between Phase I and Phase II.

6.2 Surface Studies

In this section I present studies of event clustering on various surfaces of the detector and detection surfaces. At event detections, charge clusters are noted as ionization charges drift in the electric field. Occasionally, and especially likely in α decays, the charge cluster is undetected, causing less position reconstruction success. The machine learning algorithm, which was trained on the fully reconstructed data set previously, is used to predict the following position reconstructions. The analyses on events with one charge cluster (1CC) are separated from the events with no charge cluster (0CC) to show the trends that differ between the two.

6.2.1 Data Cuts

The data sets used in these Surface Studies are cut the same way as previously outlined, but have either the 1CC restriction or the 0CC restriction on them. Once generated, they were reconstructed with the trained DTR algorithm from the same fully reconstructed α decay event set which was discussed earlier. Because the DTR was trained on a similarly cut set of data (α cuts in similar volume regions), it should perform well on this data. After the event data collection, the events are split into different sets which we analyze separately. There are two main event selections here:

1. Inside/outside fiducial volume
2. Inside/outside R=172.0 mm

The first deals with "bulk" events which are in the bulk of the detector, and not near or on the anodes or cathode. Being "inside" the fiducial volume is analogous to being a bulk event. Being "outside" the fiducial volume means the events are near the anodes or cathode.

The second deals with the round wall of the cylindrical detector. Interestingly, in neither 1CC or 0CC events were there any reconstructed (or otherwise) R values that put the event outside that radius. The collected data that was used to train the decision tree did not have any events that exceeded R= 172.0 mm, which completely biased the predictions to inside that volume.

6.2.2 1CC

Here I present the 3D distribution of events outside the fiducial z (see Figure 13, pg. 19). The clustering on the anodes and cathodes is expected, with a slight bias for the cathode events at z= 0, which is also expected. Any positively charged ions will drift to the cathode and decay there, and these plots do include any α decay parents, not only ^{218}Po.

The histogram (see Figure 14, pg. 20) shows a normal distribution of z positions. This is not unexpected, as 1CC events should have a strong reconstruction before the machine learning algorithm.

6.2.3 0CC

In the 0CC events, the reconstructions visualized below are heavily reliant on the machine learning algorithm to fill in the position. Below are the 0CC events as reconstructed by the DTR trained on fully reconstructed Phase II events. The 0CC figures show more interesting features, although, because of this, they highlight the need for a larger baseline of events to begin with in order to show strong trending.

First, the 3D distribution of 0CC events outside the fiducial z (see Figure 16, pg. 21). Once again, the slight biasing towards the cathode is visible. The top-down view seems to be evenly distributed as well, which is expected for events outside the fiducial z.

Next is the 3D distribution of 0CC events *inside* the fiducial z (see Figure 17, pg. 22). With these events, we might expect a slight biasing towards the walls of the detector due to the ions (since we have cut out the anodes and cathode). In the top-down view, this feature is noticeable, though more events would increase any ability to see these features.

The histogram of z positions for 0CC events is extremely irregular, where it would be expected to be not much more irregular than the 1CC histogram.

7 Conclusion

Understanding the way the EXO-200 detector behaves internally is important in confidently measuring and reconstructing data. In a detector optimized for $0\nu\beta\beta$ decays, α decays are difficult to get full reconstructions for due to their energy vs. scintillation footprint. Those α decays come mainly from contaminants within the LXe or from pieces of the detector apparati. This combination of causes makes them interesting in terms of detector-related studies that can be done, but also creates a need for a way to reconstruct these α decays accurately.

Erica Smith [16] presents the framework for a machine learning based reconstruction algorithm for these α decays in question. In the interest of a Phase II analysis with the same suite of tools, I show that the reconstruction seems strong still, though there is a deficit of events that needs to be overcome to be able to draw strong statistics from the Phase II data.

In the future, these tools can be used to monitor the effects of detector changes and α decays on the detector, both in ion movement and possible charging on the edges of the detector. As nEXO comes online, the α decays will still offer a valuable insight into detector optimization and understanding.

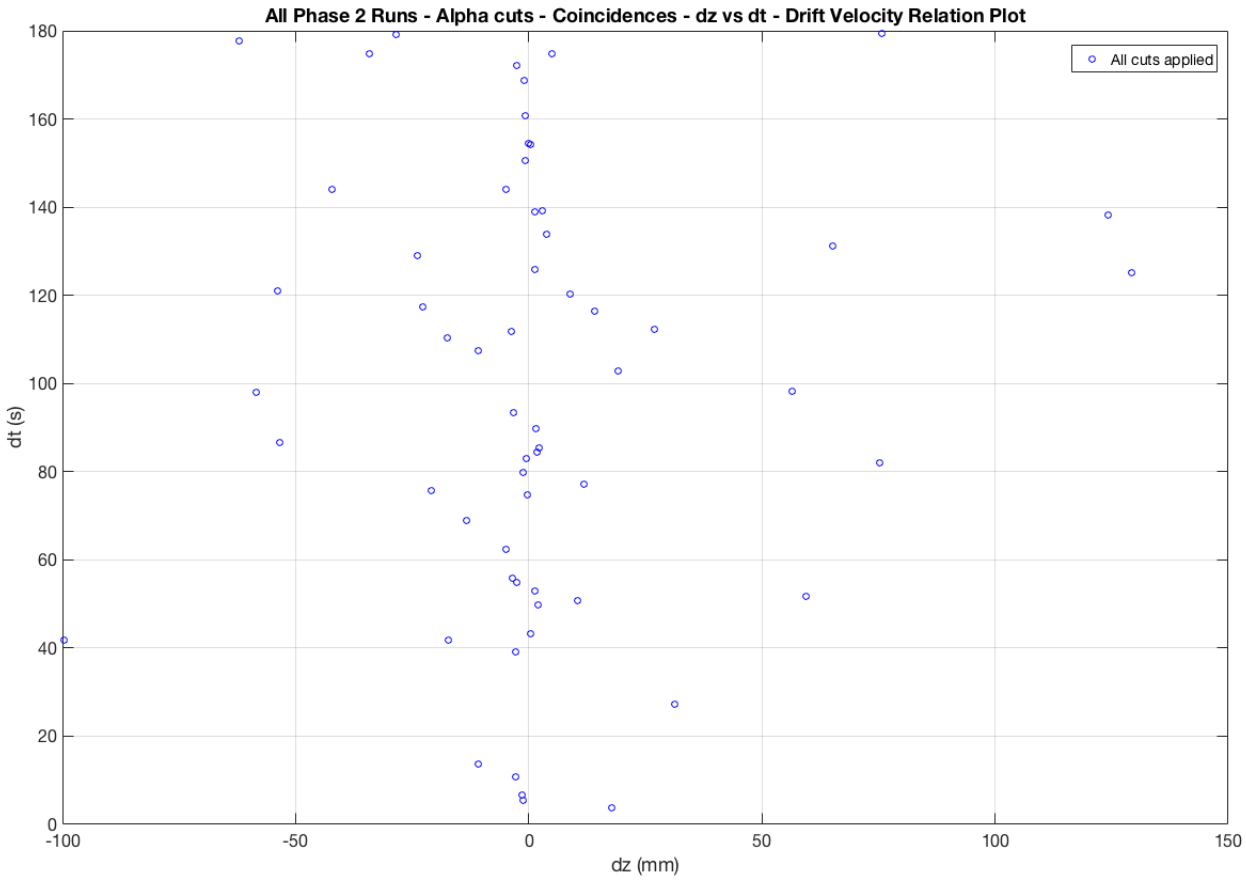

Figure 8: ^{218}Po drift time versus drift distance (61 events passing cuts)

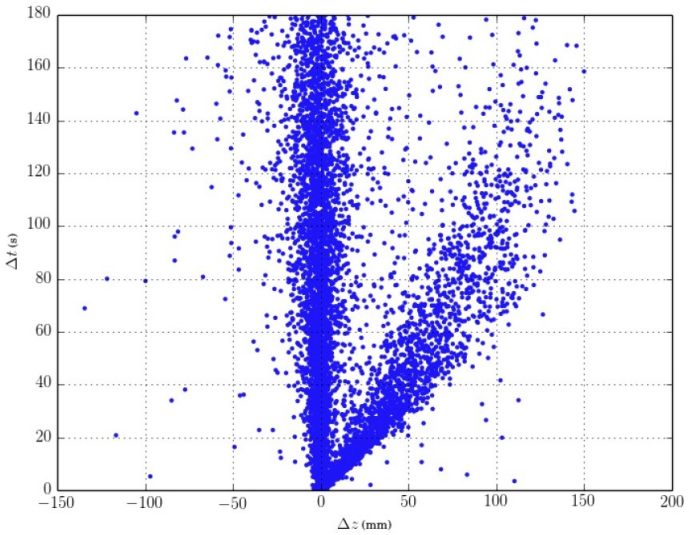

Figure 9: ^{218}Po drift time versus drift distance (6785 events passing cuts) - from Erica Smith [16]

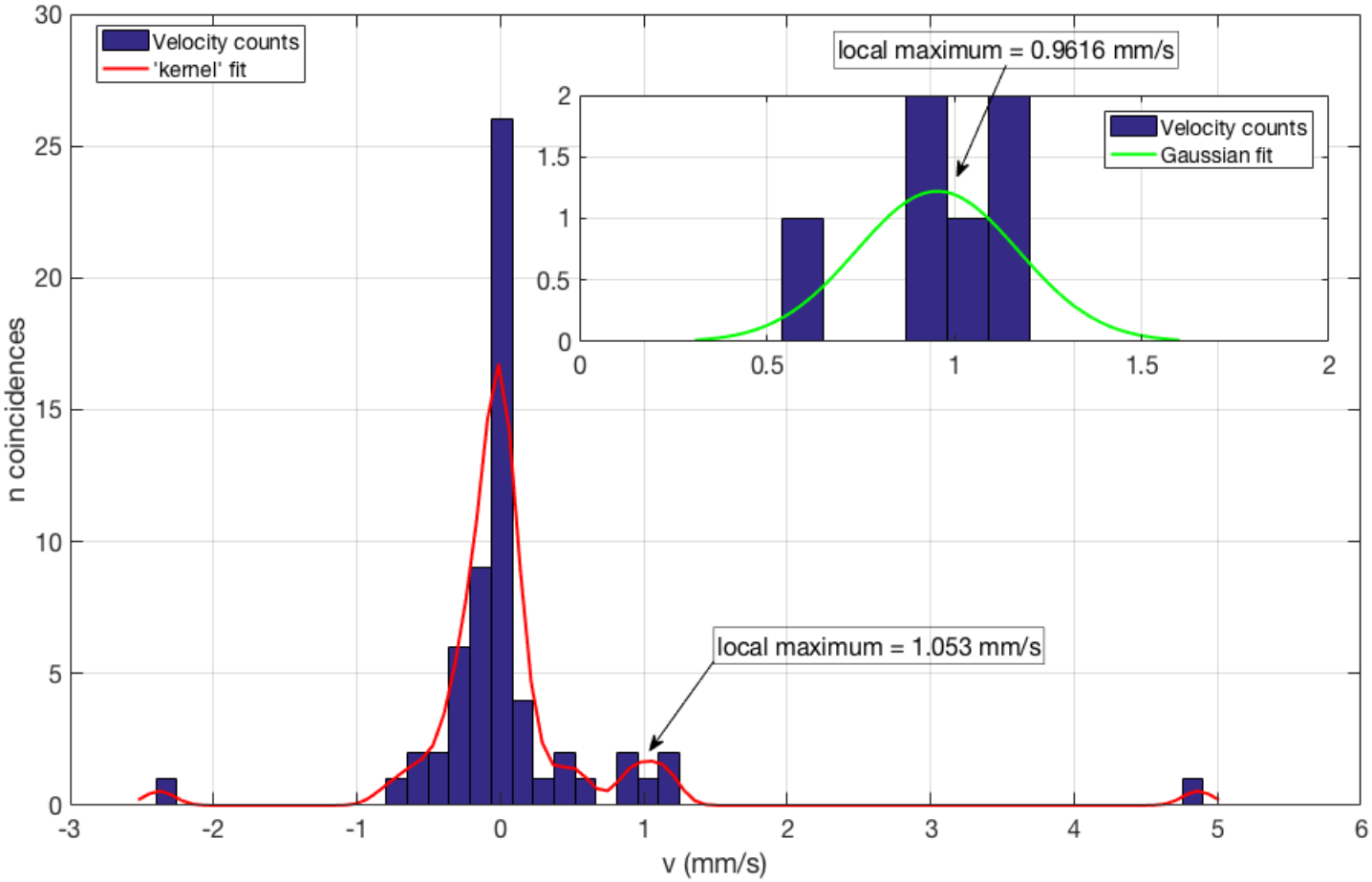

Figure 10: Mean velocity of ^{218}Po (atoms and ions).
Inset is zoomed into ion peak. $1\sigma = 0.2156$ (6 events)

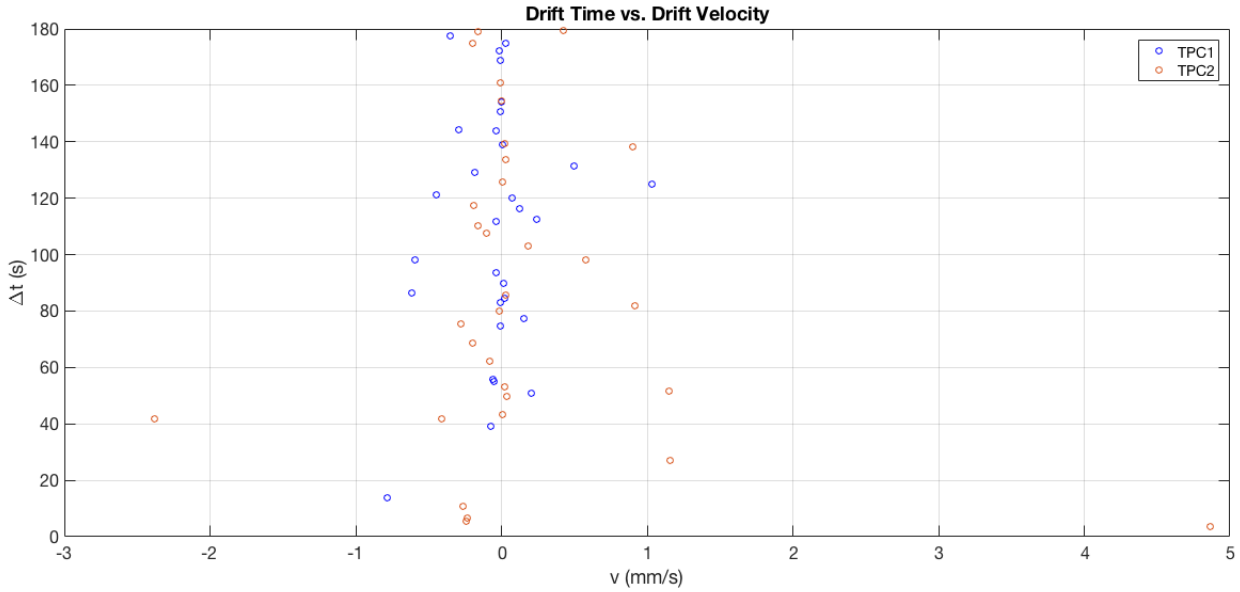

Figure 11: ^{218}Po drift time versus drift velocity

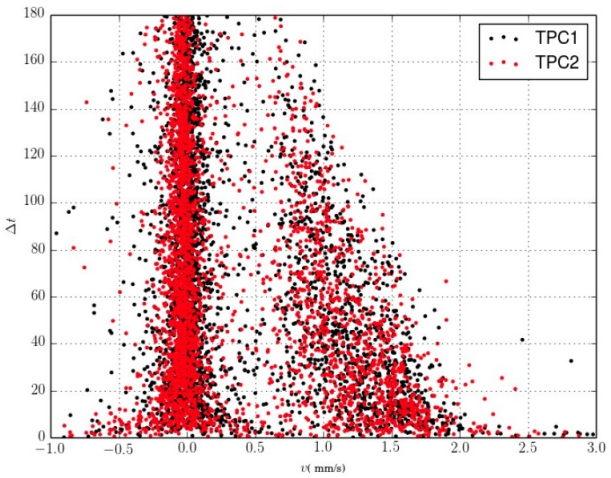

Figure 12: ^{218}Po drift time versus drift velocity - from Erica Smith [16]

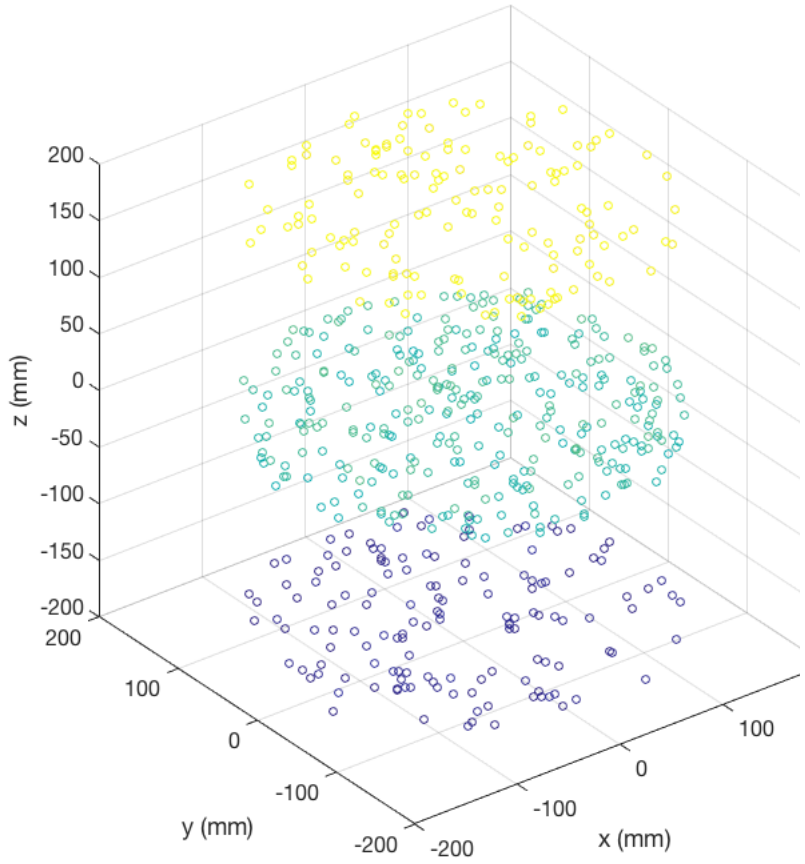

(a) 3D Representation

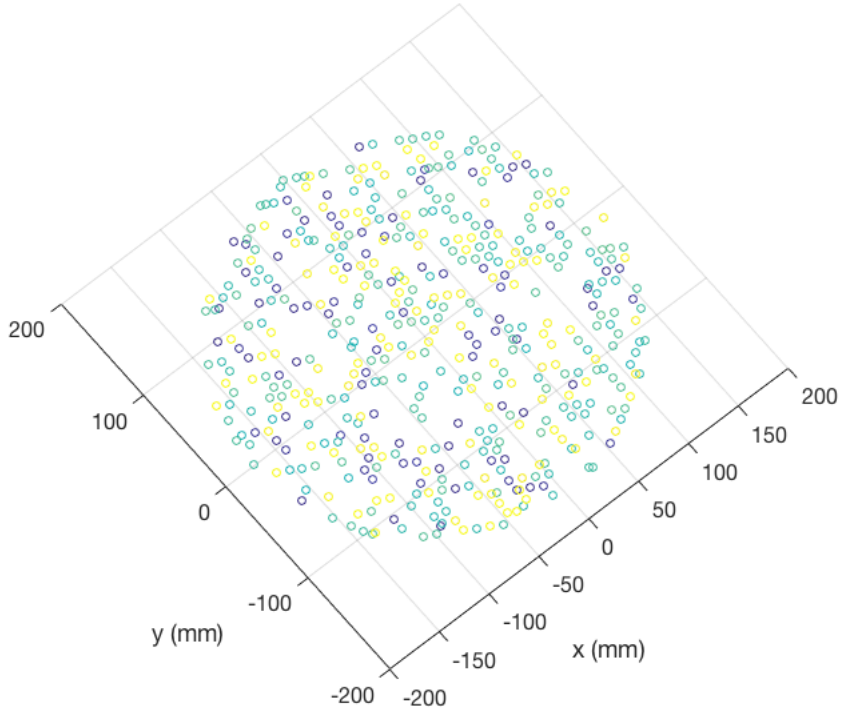

(b) Top-down view

Figure 13: 1CC events outside fiducial z

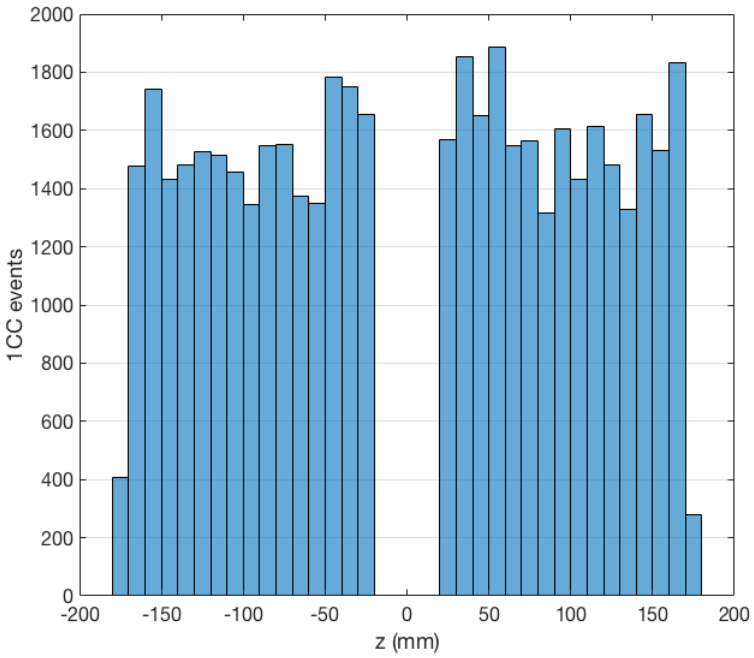

Figure 14: Histogram showing z distribution of all 1CC events inside fiducial z

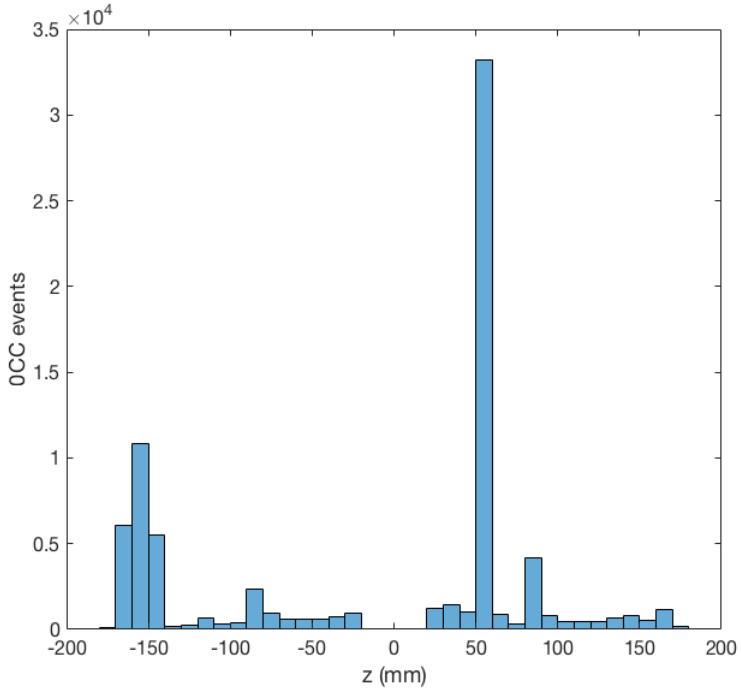

Figure 15: Histogram showing a z distribution of all 0CC events inside fiducial z

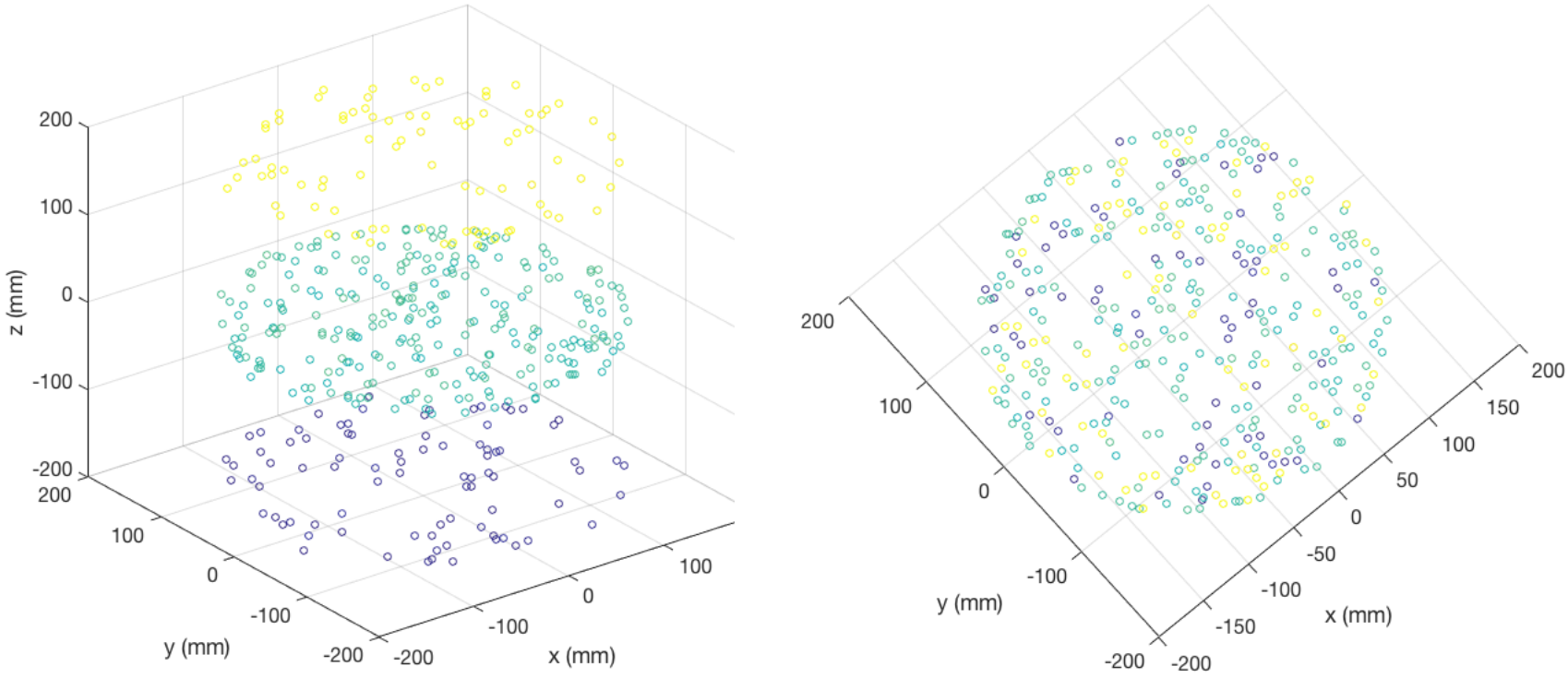

(a) 3D Representation

(b) Top-down view

Figure 16: 0CC events outside fiducial z

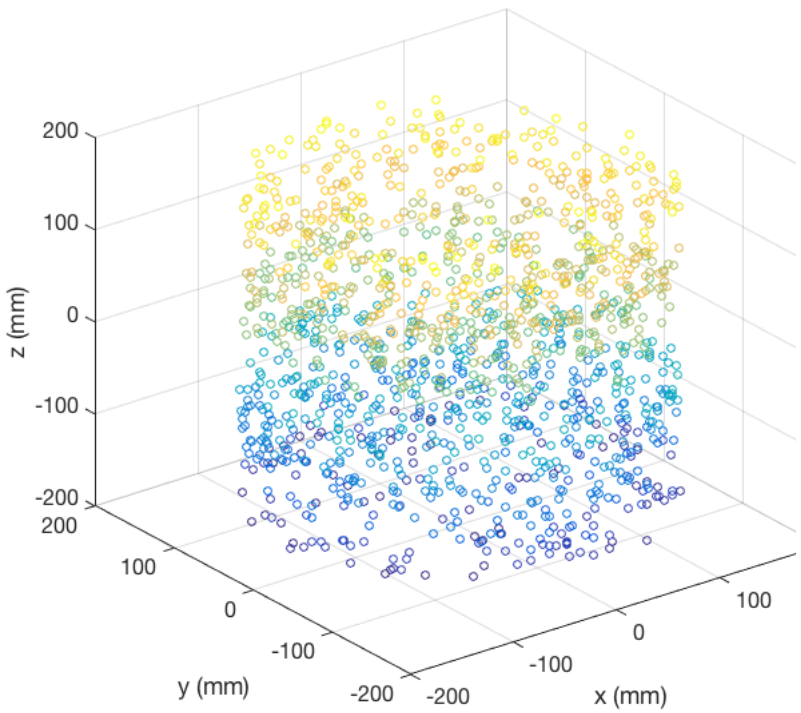

(a) 3D Representation

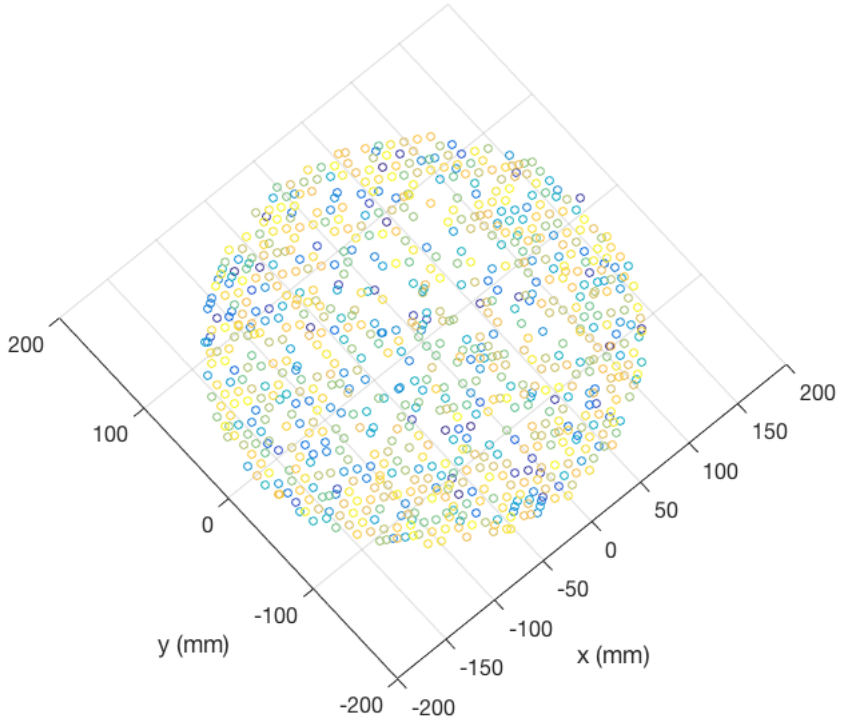

(b) Top-down view

Figure 17: 0CC events inside fiducial z

References

[1] N. Ackerman et al. (EXO-200 Collaboration) *Observation of Two-Neutrino Double-Beta Decay in ^{136}Xe with the EXO-200 Detector*. Phys. Rev. Let. 107, 212501. 17 November 2011. [arXiv:1108.4193]

[2] J. B. Albert et al. (EXO-200 Collaboration) *An improved measurement of the $2\nu\beta\beta$ half-life of ^{136}Xe with EXO-200*. Phys. Rev. C 89, 015502. 29 January 2014. [arXiv:1306.6106v4]

[3] J. B. Albert et al. (EXO-200 Collaboration) *Cosmogenic Background to $0\nu\beta\beta$ in EXO-200*. 16 April 2016. [arXiv:1512.06835v2]

[4] J. B. Albert et al. (EXO-200 Collaboration) *Measurements of the ion fraction and mobility of α- and β-decay products in liquid xenon using the EXO-200 detector*. Phys. Rev. C 92:045504. 28 October 2015. [arXiv:1506.00317v2]

[5] J. B. Albert et al. (EXO-200 Collaboration) *Search for Majorana neutrinos with the first two years of EXO-200 data*. Nature 510, 229-234. 12 June 2014. [arXiv:1402.6956v2]

[6] J. B. Albert et al. (EXO-200 Collaboration) *Search for Neutrinoless Double-Beta Decay with the Upgraded EXO-200 Detector*. Phys. Rev. Lett. 120, 072701. 26 Feb 2018. [arXiv:1707.08707v2]

[7] M. Auger et al. (EXO-200 Collaboration) *The EXO-200 detector, part I: Detector design and construction* 2012. [arXiv:1202.2192]

[8] M C Chen. *Neutrinoless double beta decay experiments*. 2015 J. Phys.: Conf. Ser. 598, 012008. `http://iopscience.iop.org/article/10.1088/1742-6596/598/1/012008/pdf`

[9] EXO-200. *About the Experiment*. 10 September 2017. `https://www-project.slac.stanford.edu/exo/about.html`

[10] Guiseppe, V. E. and Elliott, S. R. and Hime, A. and Rielage, K. and Westerdale, S. *A Radon Progeny Deposition Model*. AIP Conf. Proc. 2011 1338:1, 95-100. Accessed: `http://icecube.wisc.edu/info/neutrinos`

[11] IceCube: South Pole Neutrino Observatory. *All About Neutrinos*. `http://icecube.wisc.edu/info/neutrinos`

[12] Jewell, Michael. *Data Processing and EXOAnalysis Overview* EXO Week, UMass Amherst. 30 June 2016. Internal communications.

[13] Jewell, Michael. *EXOProcessedData – Phase I and Phase II Data Locations* EXO Confluence Wiki. Internal communications. `https://confluence.slac.stanford.edu/display/exo/EXOProcessData+--+Phase+I+and+Phase+II+Data+Locations`

[14] Johnson, Tessa. *How Does nEXO Work?*. `https://nexo.llnl.gov/content/assets/docs/HowDoesnEXOWork_Final_Print.pdf`

[15] M Redshaw, et al. *Mass and Double-Beta-Decay Q Value of ^{136}Xe* Phys. Rev. Lett. 98, 053003. 2 February 2007.

[16] Smith, Erica. *Characterization of Radon Progeny in EXO-200 Using Machine Learning Algorithms*. Drexel University, Philadelphia, PA. February 2016.

[17] Stanford University, for the U.S. Department of Energy Office of Science. *EPP - Elementary Particle Physics: Enriched Xenon Observatory*. https://epp.slac.stanford.edu/research/enriched-xenon-observatory

[18] Stanford University, for the U.S. Department of Energy Office of Science. *SLAC: National Accelerator Laboratory*. https://www6.slac.stanford.edu

[19] Stewart, Danielle. *Double Beta Decay*. University of Warwick, UK. ePortfolio. https://warwick.ac.uk/study/csde/gsp/eportfolio/directory/crs/phsgbu/research/phdresearch/theory/betadecay/double/

[20] P. Vogel and A. Piepke. *69. Neutrinoless Double-β decay*. 1 December, 2017. http://pdg.lbl.gov/2017/reviews/rpp2016-rev-neutrinoless-double-beta-decay.pdf

[21] Wikipedia. *Double Beta Decay*. https://en.wikipedia.org/wiki/Double_beta_decay

[22] Sci-kit learn. *scikit-learn 0.19.1 documentation*